



HAL
open science

15 Deoxi- Δ -Prostaglandin j is a tubulin-binding agent that destabilizes microtubules and induces mitotic arrest

Claudia Cocca, Jorge Dorado, Enrique Calvo, Juan Antonio López, Angel Santos, Ana Perez-Castillo

► To cite this version:

Claudia Cocca, Jorge Dorado, Enrique Calvo, Juan Antonio López, Angel Santos, et al.. 15 Deoxi- Δ -Prostaglandin j is a tubulin-binding agent that destabilizes microtubules and induces mitotic arrest. *Biochemical Pharmacology*, 2009, 78 (10), pp.1330. 10.1016/j.bcp.2009.06.100 . hal-00522544

HAL Id: hal-00522544

<https://hal.science/hal-00522544>

Submitted on 1 Oct 2010

HAL is a multi-disciplinary open access archive for the deposit and dissemination of scientific research documents, whether they are published or not. The documents may come from teaching and research institutions in France or abroad, or from public or private research centers.

L'archive ouverte pluridisciplinaire **HAL**, est destinée au dépôt et à la diffusion de documents scientifiques de niveau recherche, publiés ou non, émanant des établissements d'enseignement et de recherche français ou étrangers, des laboratoires publics ou privés.

Accepted Manuscript

Title: 15 Deoxi- $\Delta^{12,14}$ -Prostaglandin j_2 is a tubulin-binding agent that destabilizes microtubules and induces mitotic arrest

Authors: Claudia Cocca, Jorge Dorado, Enrique Calvo, Juan Antonio López, Angel Santos, Ana Perez-Castillo



PII: S0006-2952(09)00592-9
DOI: doi:10.1016/j.bcp.2009.06.100
Reference: BCP 10248

To appear in: *BCP*

Received date: 29-4-2009
Revised date: 18-6-2009
Accepted date: 24-6-2009

Please cite this article as: Cocca C, Dorado J, Calvo E, López JA, Santos A, Perez-Castillo A, 15 Deoxi- $\Delta^{12,14}$ -Prostaglandin j_2 is a tubulin-binding agent that destabilizes microtubules and induces mitotic arrest, *Biochemical Pharmacology* (2008), doi:10.1016/j.bcp.2009.06.100

This is a PDF file of an unedited manuscript that has been accepted for publication. As a service to our customers we are providing this early version of the manuscript. The manuscript will undergo copyediting, typesetting, and review of the resulting proof before it is published in its final form. Please note that during the production process errors may be discovered which could affect the content, and all legal disclaimers that apply to the journal pertain.

1 **15 DEOXI- $\Delta^{12,14}$ -PROSTAGLANDIN J₂ IS A TUBULIN-BINDING AGENT**
2 **THAT DESTABILIZES MICROTUBULES AND INDUCES MITOTIC**
3 **ARREST.**

4 **Claudia Cocca^{1,2*}, Jorge Dorado^{1*}, Enrique Calvo³, Juan Antonio López³, Angel**
5 **Santos⁴, and Ana Perez-Castillo¹.**

6
7 Abbreviated title: Mitotic arrest induced by 15d-PGJ₂.

8
9
10 ¹Instituto de Investigaciones Biomédicas, Consejo Superior de Investigaciones
11 Científicas-Universidad Autónoma de Madrid and Centro de Investigación Biomédica
12 en Red sobre Enfermedades neurodegenerativas (CIBERNED, 28029-Madrid, Spain.

13 ²Present address: Laboratorio de Radioisótopos. Facultad de Farmacia y Bioquímica.
14 Universidad de Buenos Aires. C1113ABB-Bs.As, Argentina.

15 ³Unidad de Proteómica. Centro Nacional de Investigaciones Cardiovasculares, Melchor
16 Fernández Almagro, 3, 29029-Madrid, Spain

17 ⁴Departamento de Bioquímica y Biología Molecular. Facultad de Medicina,
18 Universidad Complutense de Madrid, 28040-Madrid, Spain.

19
20
21
22 *Both authors contributed equally to this work

23
24
25 Address correspondence to: Ana Perez-Castillo. Instituto de Investigaciones
26 Biomédicas, Consejo Superior de Investigaciones Científicas-Universidad Autónoma de
27 Madrid. Arturo Duperier, 4. 28029-Madrid. Spain. Phone: 34-91-5854436, Fax: 34-91-
28 5854401, e-mail: aperez@iib.uam.es or to: Angel Santos. Departamento de
29 Bioquímica y Biología Molecular, Facultad de Medicina, Universidad Complutense,
30 Madrid. Spain. Phone: 34-91-3941446. Fax: 34-91-3941691, e-mail:
31 piedras3@med.ucm.es
32
33
34
35
36
37
38
39
40
41
42
43
44
45
46
47
48
49
50
51
52
53
54
55
56
57
58
59
60
61
62
63
64
65

ABSTRACT:

1
2 15-deoxy- $\Delta^{12,14}$ -prostaglandin J₂ (15d-PGJ₂) is known to play an important role in
3
4 the pathophysiology of carcinogenesis, however the molecular mechanisms underlying
5
6 these effects are not yet fully understood. Recently, we have shown that 15d-PGJ₂ is a
7
8 potent inducer of breast cancer cell death and that this effect is associated with a
9
10 disruption of the microtubule cytoskeletal network. Here, we show that treatment of the
11
12 MCF-7 breast cancer cell line with 15d-PGJ₂ induces an accumulation of cells in the
13
14 G₂/M compartment of the cell cycle and a marked disruption of the microtubule
15
16 network. 15d-PGJ₂ treatment causes mitotic abnormalities that consist of failure to form
17
18 a stable metaphase plate, incapacity to progress through anaphase, and failure to
19
20 complete cytokinesis. 15d-PGJ₂ binds to tubulin through the formation of a covalent
21
22 adduct with at least four cysteine residues in α - and β -tubulin, as detected by hybrid
23
24 triple-quadrupole mass spectrometry analysis. Overall, these results support the
25
26 hypothesis that microtubule disruption and mitotic arrest, as a consequence of the
27
28 binding of 15d-PGJ₂ to tubulin, can represent one important pathway leading to breast
29
30 cancer cell death.
31
32
33
34
35
36
37
38
39
40

41 Keywords: 15d-PGJ₂, cell death, cytoskeleton, mitosis, tubulin, cancer.
42
43
44
45
46
47
48
49
50
51
52
53
54
55
56
57
58
59
60
61
62
63
64
65

INTRODUCTION

1
2 Cyclopentenone prostaglandins are potent bioactive molecules involved in regulating
3
4 many physiological as well as pathological processes [1, 2]. Some of these
5
6 prostaglandins have been shown to induce cell cycle arrest and apoptosis in a number of
7
8 cancer cell types [3]. In particular, the terminal derivative of prostaglandin J₂
9
10 metabolism, 15-deoxy- $\Delta^{12,14}$ -prostaglandin J₂ (15d-PGJ₂), is emerging as the most potent
11
12 antineoplastic agent of this class of prostaglandins. Anticancer activity of 15d-PGJ₂ has
13
14 been reported both in vitro and in vivo in a multiplicity of tissues including breast,
15
16 prostate, colon, lung, brain, skin, and lymphoid [4-11]. However, the mechanism of
17
18 15d-PGJ₂ antineoplastic activity has not been fully elucidated as yet.
19
20
21
22
23
24
25
26

27 Although 15d-PGJ₂ was identified as a high-affinity natural ligand for peroxisome
28
29 proliferators-activated receptor (PPAR) γ [12], it is now thought to exert its effects
30
31 through PPAR γ -dependent and -independent mechanisms. Among these PPAR γ -
32
33 independent mechanisms are pathways that operate through NF- κ B and AP1, and other
34
35 signal transducers and activators of transcription [13-16]. 15d-PGJ₂ has also been
36
37 reported to induce apoptosis of several types of cancer cells and normal cells
38
39 independently of PPAR γ activation including breast cancer cells, dendritic cells, and
40
41 hepatic myofibroblasts [17-19]. For example, hepatic myofibroblasts do not express
42
43 PPAR γ , but still undergo apoptosis when exposed to 15d-PGJ₂. We have also reported
44
45 that 15d-PGJ₂ is a potent inhibitor of mitochondrial function through PPAR γ -
46
47 independent means [20].
48
49
50
51
52
53
54
55
56

57 We have recently shown that 15d-PGJ₂ inhibits neoplastic breast cancer cell
58
59 proliferation, induces apoptosis, and disrupts microtubule (MT) assembly, suggesting
60
61
62
63
64
65

1 that the anti-neoplastic effects of 15d-PGJ₂ can be triggered by multiple mechanisms,
2 one of them probably involving MT dynamics [8]. Microtubules are the principal
3 components of the cytoskeleton network of eukaryotic cells and have been shown to be
4 involved in various cellular functions, including cell division, cytokinesis, maintenance
5 of cell morphology, and signal transduction [21, 22] Microtubules are intracellular,
6 filamentous, polymeric structures composed of two structurally similar protein subunits,
7 namely, α - and β -tubulin (molecular weight, 50 kDa each). During mitosis,
8 microtubules undergo rapid polymerization and depolymerization to enable movement
9 of chromosomes. As cell division approaches metaphase, microtubules are disrupted
10 and form a spindle surrounding the centrosome, thereby facilitating chromosomal
11 alignment on the metaphase plate. In this process, tubulin subunits freely exchange on
12 the microtubules. If such free exchange of tubulin subunits is disrupted, the mitotic
13 spindle is compromised and the cell cannot divide. Certain drugs have already been
14 discovered which bind tubulin (e.g., Vinca alkaloids and the colchicine-site binders),
15 thereby preventing them from being incorporated into growing microtubules. As a
16 consequence cells undergoing division, and particularly those cells showing rapid
17 division (i.e., cancer cells), are killed. Thus, in the field of antineoplastic chemotherapy,
18 anti-microtubule agents constitute an important class of compounds, with broad activity
19 both in solid tumors and in hematological malignancies [21, 23, 24].

20 Here, we show that upon treatment with 15d-PGJ₂, MCF-7 breast cancer cell line
21 arrest at the G₂/M phase of the cell cycle. 15d-PGJ₂ also causes a depolymerization of
22 the microtubule network and inhibits assembly of purified tubulin in vitro, probably due
23 to the covalent modification of at least four cysteine residues in polymerized α - and β -
24 tubulin. This microtubule disorganization is accompanied by mitotic abnormalities and

1 incapacity to progress through anaphase. This study identifies tubulin as a molecular
2 target of the pro-apoptotic 15d-PGJ₂ compound.
3
4
5
6
7
8
9
10
11
12
13
14
15
16
17
18
19
20
21
22
23
24
25
26
27
28
29
30
31
32
33
34
35
36
37
38
39
40
41
42
43
44
45
46
47
48
49
50
51
52
53
54
55
56
57
58
59
60
61
62
63
64
65

Accepted Manuscript

MATERIALS AND METHODS

1
2 *Cell culture.* MCF-7 human mammary epithelial cells were grown as previously
3
4 described [7]. For microscopy experiments cells were grown on glass coverslips.
5
6
7 Experimental cultures were stimulated with the appropriate ligand, as indicated.
8
9

10
11 *Antibodies.* Pericentrin rabbit polyclonal antibody was from Covance (Berkeley,
12
13 California). Mouse monoclonal anti- α -tubulin (Clone DM 1A) and anti- β -tubulin
14
15 (Clone SDL.3D10) antibodies were from Sigma (St Louis, MO). Biotin goat polyclonal
16
17 and Alexa secondary antibodies were from Vector Laboratories (Burlingame, USA)
18
19
20
21
22

23
24 *Cell cycle analysis.* MCF-7 cells were treated with 10 μ M 15dPG-J₂ (Cayman
25
26 Chemical, MI, USA) or 30 μ M rosiglitazone (Cayman Chemical, MI, USA) in regular
27
28 RPMI medium for 24 h. Cells were then fixed in 70% ethanol/PBS, pelleted and
29
30 resuspended in buffer containing 10 μ g/ml RNase A and 0.01 mg/ml propidium iodide.
31
32
33 Cell cycle distribution was determined by flow cytometric analysis utilizing a Cyan
34
35 MLE-R Cytometer (DAKO-Cytomation, Glostrup, Denmark). Data analysis was
36
37 performed using the Summit Software (DAKO).
38
39
40
41
42

43
44 *In vitro tubulin polymerization assay.* In vitro tubulin assembly was evaluated using the
45
46 HTS-Tubulin Polymerization Assay Kit (Cytoskeleton, Denver, CO), according to the
47
48 manufacturer's instructions. Absorbance readings were taken at 340 nm every 30 s for 1
49
50
51 h, using a Varioscan (Thermo Electron Corporation) plate reader and Skanit 2.0
52
53
54 Research Edition.
55
56
57
58
59
60
61
62
63
64
65

1
2
3
4
5
6
7
8
9
10
11
12
13
14
15
16
17
18
19
20
21
22
23
24
25
26
27
28
29
30
31
32
33
34
35
36
37
38
39
40
41
42
43
44
45
46
47
48
49
50
51
52
53
54
55
56
57
58
59
60
61
62
63
64
65

Separation of soluble and polymerized tubulins. Separation of soluble and polymerized tubulins was carried out as described by Minotti et al [25]. Briefly, 12 h after 15d-PGJ₂ (10 μM) or rosiglitazone (30 μM) treatment, MCF-7 cells were lysed using 120 μl of microtubule-stabilizing buffer [20 mM Tris-HCl (pH 6.8), 1 mM MgCl₂, 2 mM EGTA, 0.5% NP-40, 2 mM PMSF, 1 mM benzamidine]. After vortexing, 120 μg of protein were centrifuged at 13,000 rpm for 15 minutes at room temperature and soluble (supernatant) and polymerized (pellet) tubulin analyzed by SDS-PAGE and immunoassay as described [8].

Biotinylated 15dPG-J₂ pull down and western blot analysis. For in vivo incorporation of 15d-PGJ₂ into α- and β-tubulin in intact cells, MCF-7 cells were incubated with 10 μM biotinylated 15d-PGJ₂ for 2 h, lysed in lysis buffer [10 mM Tris-HCl (pH 7.5), 0.1 mM EDTA, 0.1 mM EGTA, 0.5% SDS, 0.1 mM 2-mercaptoethanol and 1mM PMSF], and biotinylated proteins were purified by adsorption onto Neutravidin beads (Pierce Biotechnology, Inc. Rockford, IL), as described by the manufacturer's. Proteins were detected by Western blot using anti-α- and anti-β antibodies, as previously described [8].

Immunofluorescence and confocal microscopy. Confocal microscopy was used to detect cytoskeleton organization. MCF-7 cells were plated on glass coverslips in 24-well cell culture plates and grown in regular medium for 12 h before switching to new medium with the corresponding treatment. Cells were then fixed for 10 min with methanol at –20°C, and washed with PBS. After one hour incubation with the appropriate primary antibody, cells were washed and incubated with DAPI, Alexa Fluor 488, Alexa Fluor 546, or Alexa Fluor 647 secondary antibodies (Molecular Probes) for 45 min at 37°C.

1
2
3
4
5
6
7
8
9
10
11
12
13
14
15
16
17
18
19
20
21
22
23
24
25
26
27
28
29
30
31
32
33
34
35
36
37
38
39
40
41
42
43
44
45
46
47
48
49
50
51
52
53
54
55
56
57
58
59
60
61
62
63
64
65

Images were acquired using a Radiance 2100 laser scanning confocal microscope (Bio-Rad, Hercules, CA) using a 60x NA 1.40 oil immersion objective (Nikon). The images were obtained using a series of 0.5 μm (depth) spaced cell fluorescent slices (Z axis). Confocal microscope settings were adjusted to produce the optimum signal-to-noise ratio. Images were collected and processed using Lasersharp 2000 and Adobe Photoshop version 8.0, respectively.

Time-Lapse microscopy. MCF-7 cells were plated and placed in a chamber in complete medium with CO_2 exchange at 37°C. Cells were imaged every 1 min for 1-2 days using a 40x objective on an inverted microscope (Zeiss Axiovert 135 TV). Images were captured on a JVC (TK-C1481EG) digital video camera. Where indicated, 10 μM 15d-PGJ₂ or 30 μM rosiglitazone were added to live microscopy media. Resulting movies were collected and processed by using image analySIS software (Soft Imaging System) and exported as Quicktime (Apple Computer, Cupertino, CA) and are shown at 7 frames per second (Supplemental videos 1-3 online).

Off line nanospray characterization of 15d-PGJ₂ by mass spectrometry. About 1 μl containing 5 μg of 15d-PGJ₂ was dissolved in 20 μl of 50% CH_3CN , 0.5% acetic acid. 5 μl was introduced into the off line nanospray medium needle and infused using the Protana nanosprayTM ion source. The 15d-PGJ₂ was ionized into a triple quadrupole mass spectrometer (4000 Q Trap LC-MS/MS hybrid system, Applied Biosystems, MDS Sciex), and data were acquired for 2 min. The needle voltage was set at 1300 V, and the declustering potential was set at 50 V to minimize in-source fragmentation. A collision energy between 25 and 30 was used to induce the fragmentation of the 15d-PGJ₂ molecule.

1
2 *Protein digestion and sample preparation for MS analysis.* Untreated or 15d-PGJ₂-
3
4 treated microtubules samples were incubated with 1 µg trypsin (Promega Sequencing
5
6 Grade) for 2 h at 37°C. Reaction mixtures were dried in vacuo and dissolved in 5%
7
8 CH₃CN, 0.5% CH₃COOH, for later MS analysis.
9
10

11
12
13
14 *Nano-HPLC and tandem triple-quadrupole MS analysis of peptides.* The tryptic
15
16 peptides from control, and 15d-PGJ₂-treated samples were injected with a Famos (LC
17
18 Packings) autosampler onto a PepMap™ C18 reversed phase micro-column (300 µm
19
20 ID x 5 mm) from LC Packings and washed to remove salts. Samples were eluted onto a
21
22 C18 reversed phase nano-column (100 µm ID x 15 cm, Teknokroma, Mediterranean sea),
23
24 which was developed with a CH₃CN gradient (5-47.5% CH₃CN over 45 min, followed
25
26 by a 1 min increase to 85.5% CH₃CN) generated by an Ultimate Nano-HPLC (LC
27
28 Packings). A flow rate of ca. 300 nl min⁻¹ was used to elute peptides from the nano-
29
30 column to a New Objective PicoTip™ emitter nano-spray needle (3000 V) in a Protana
31
32 nanospray ion source, and ions were analyzed with the 4000 Q-Trap system. In the
33
34 enhanced resolution mode, the linear ion trap was scanned at m/z 250/s, and the ion of
35
36 interest was selected in Q1 by precursor ion scanning. N₂ was used as the curtain (value
37
38 of 15) and collision gas (set to high).
39
40
41
42
43
44
45
46
47
48

49 *Multiple Reaction Monitoring (MRM).* 15d-PGJ₂-bound tryptic peptides from treated
50
51 and untreated microtubules were analyzed in the MRM mode. Q1 was set on the m/z
52
53 corresponding to charged parent ions from masses 1, 2, 3, and 4 previously observed
54
55 (see results; m/z at 644.4, 662.9, 726.4, and 989.9, respectively), and Q3 was set on
56
57 specific fragment ions for each parent mass (m/z at 482.3 corresponding to y₄ fragment
58
59
60
61
62
63
64
65

1 ion for mass 1, m/z at 948.2 corresponding to 15d-PGJ₂-modified y6 fragment ion for
2 mass 2, m/z at 841.4 corresponding to y7 fragment ion for mass 3, and m/z 1326.1
3
4 corresponding to doubly-charged, y25 fragment ion for mass 4; Supplementary Fig. 2).
5
6 Collision energy was set to 30 eV.
7
8
9

10
11 *MS data analysis.* All the chromatograms and MS/MS spectra from the 4000 Q Trap
12 System were analyzed with Analyst 1.4.1 software (Applied Biosystems). Analyses of
13
14 15d-PGJ₂-binding to microtubules by MS were repeated with two independent samples.
15
16
17
18
19
20

21 *Statistical analysis.* The data shown are the means±s.d. of at least three independent
22 experiments. Statistical comparisons for significance between cells with different
23
24 treatments were performed using the Student's t test.
25
26
27
28
29
30
31
32
33
34
35
36
37
38
39
40
41
42
43
44
45
46
47
48
49
50
51
52
53
54
55
56
57
58
59
60
61
62
63
64
65

RESULTS

15d-PGJ₂ arrests the cell cycle at G₂/M phase and causes a disruption of MCF-7 microtubule network. To determine the effect of 15d-PGJ₂ on cell cycle, exponentially growing MCF-7 cells were treated with 15d-PGJ₂ for 24 h and their cell cycle progression was followed by fluorescence activated cell sorting analysis. Fig. 1 demonstrates that treatment with 15d-PGJ₂ led to significant increased numbers of G₂/M phase cells, compared with non-treated control cells. On the contrary, the percentage of cells in the G₂/M cell cycle state did not differ markedly between control and MCF-7 cells treated with rosiglitazone (RSG), a specific synthetic PPAR γ agonist. Nocodazole, a potent anti-microtubule agent capable of rapidly depolymerizing the MT network, was used as control [26].

It has been very well documented that MT inhibitors are known to arrest cells in G₂/M phase and induce cell death [21, 22]. Based on this observation, and our previous results [8], we then reasoned that the induction of G₂/M arrest by 15d-PGJ₂ could be attributed to the disruption of the cytoskeleton. To test this hypothesis, we first examined whether 15d-PGJ₂ could directly affect the organization of the MT network of MCF-7 cells in the interphase phase. To this end, MCF-7 cells were treated with 15d-PGJ₂, rosiglitazone, or nocodazole and the MT network was visualized by immunofluorescence after 12 h of incubation. In control cells, the MT network exhibited normal arrangement with MT seen to traverse intricately throughout the cell and a normal compact rounded nucleus (Fig. 2A). In contrast, 15d-PGJ₂ treatment led to a dramatic disruption of the MCF-7 cytoskeleton, producing a diffuse MT network. These effects, which are similar to those exerted by nocodazole, were not observed after

1
2
3
4
5
6
7
8
9
rosiglitazone treatment. The multiple-dot pericentrin pattern obtained is characteristic of
10
11
12
13
14
15
16
17
18
19
20
21
22
23
24
25
26
27
28
29
30
31
certain breast cancer cell lines [27] and was corroborated by γ -tubulin staining (data not
shown).

To further demonstrate that 15d-PGJ₂ could promote MT depolymerization *in vivo*,
we next investigated the fraction of free and polymerized α -tubulin in control and 15d-
PGJ₂-treated MCF-7 cells, specifically by harvesting the cells in a MT-stabilizing buffer
and performing differential sedimentation. Our results indicate that the amount of
polymerized α -tubulin in the pellet fraction was significantly decreased 12 h after
treatment of MCF-7 cells with 15d-PGJ₂, when compared with basal cultures (Fig 2B,
C). In contrast, we could not observe any decrease in polymerized tubulin after
treatment with rosiglitazone, in comparison with control non-treated MCF-7 cells.

Mitotic abnormalities following 15d-PGJ₂ treatment. Microtubule targeting agents are
known to arrest the cell cycle in early mitosis i.e. prometaphase/metaphase. Therefore,
we next investigated the effect of 15d-PGJ₂ on MCF-7 cell division. We first examined
mitotic figures in MCF-7 cells treated or not with 15d-PGJ₂ for 24 h, fixed and co-
stained with DAPI and anti- α -tubulin and anti-pericentrin antibodies to monitor DNA,
the mitotic spindle, and the centrosomes, respectively. Cell morphology and the
percentage of cells at different stages of mitosis and cytokinesis were determined using
a confocal microscope. Control cells with no added 15d-PGJ₂ rounded up at the
beginning of mitosis and split into two symmetrical daughter cells as expected (Fig.
3A). In contrast, although 15d-PGJ₂-treated cells developed spindle-like structures (Fig.
3B), the MT fibers generally lack the organization observed in control cells. Also, in the
cultures treated with 15d-PGJ₂, we could not detect any cell proceeding to either

1
2
3
4
5
6
7
8
9
10
11
12
13
14
15
16
17
18
19
20
21
22
23
24
25
26
27
28
29
30
31
32
33
34
35
36
37
38
39
40
41
42
43
44
45
46
47
48
49
50
51
52
53
54
55
56
57
58
59
60
61
62
63
64
65

anaphase or telophase/cytokinesis and these cells displayed distinct signs of arrest in the metaphase stage of mitosis as the nuclear membrane has disappeared and the chromatin was condensed. The major changes, however, were the complete absence of anaphase and telophase cells and the large increase in the percentage of metaphase cells exhibiting metaphase plates with incomplete chromosome alignment, following 15d-PGJ₂ treatment. Cells with such characteristics were unable to undergo cytokinesis. The stage of mitosis at which the block occurred was further determined by counting the number of cells at each stage of mitosis. As shown in Fig. 3C, in the 15d-PGJ₂-treated MCF-7 cells, the number of cells in anaphase and telophase/cytokinesis decreased to zero, indicating a block specifically at the transition from metaphase to anaphase. These results suggest that 15d-PGJ₂ acts as a mitotic inhibitor.

Time-lapse microscopy was utilized to characterize the fate of MCF-7 cells treated with 15d-PGJ₂ and rosiglitazone (Fig. 4 and Supplementary Videos 1-3 online). We have found that the majority of control non-treated cells undergo cell division within 80 to 90 min (Fig. 4 and Supplementary Video 1 online). Non-treated cells were able to segregate chromosomes, proceed through anaphase, initiate furrow formation and elongate the midbodies. Eventually the cells segregate and flatten out. However, the majority of 15d-PGJ₂-treated cells took 3 h or longer for a significant number of cells to proceed to metaphase. During that time, cells could go through the nuclear envelope breakdown but they were unable to form a stable metaphase plate with all the chromosomes aligned to it and eventually proceed to anaphase. The single prominent phenotype associated with 15d-PGJ₂ treatment was failure to complete cytokinesis. After more than 7 h in a “metaphase-like” stage, cells eventually shriveled and died (Fig. 4 and Supplementary Video 2 online). When MCF-7 cells were treated with

1
2
3
4
5
6
7
8
9
10
11
12
13
14
15
16
17
18
19
20
21
22
23
24
25
26
27
28
29
30
31
32
33
34
35
36
37
38
39
40
41
42
43
44
45
46
47
48
49
50
51
52
53
54
55
56
57
58
59
60
61
62
63
64
65

rosiglitazone, no significant differences in the process of mitosis were observed (Fig. 4 and Supplementary Video 3 online). Cells treated with rosiglitazone were able to complete mitosis within a period of time similar to the one observed for control non-treated cells. When taken together with the images shown in Fig. 3, these results provide compelling evidence that treatment of MCF-7 cells with 15d-PGJ₂ results in failure of cell division through arrested metaphase.

Effect of 15d-PGJ₂ on tubulin polymerization in vitro. Because 15d-PGJ₂ markedly disrupted the cellular MT network, we tested whether 15d-PGJ₂ could directly affect tubulin, the main component of this network. An in vitro biochemical tubulin polymerization assay was carried out to investigate the activity of 15d-PGJ₂ on MT function. Results presented in Fig. 5 shows that 15d-PGJ₂ significantly inhibited the polymerization of tubulin, similar to the effect elicited by nocodazole, a well-known MT destabilizer. On the contrary, the addition of paclitaxel, in agreement with previous reports, favors tubulin polymerization. In contrast, rosiglitazone was found to have a negligible effect upon the polymerization of tubulin in vitro, relative to the vehicle control (data not shown), in agreement with its lack of effect upon the cellular MT network. This again, distinguishes the mechanism of action of both PPAR γ ligands and suggests that the effects of 15d-PGJ₂ are independent of PPAR γ activation. These data suggest that 15d-PGJ₂ could bind directly to tubulin and thereby prevent its polymerization and identify tubulin as a molecular target of 15d-PGJ₂.

The possibility that 15d-PGJ₂ could directly bind to, both α - and β -tubulin in vivo was investigated by using a biotinylated 15d-PGJ₂ derivative. To this end, we first analyzed the incorporation of biotinylated 15d-PGJ₂ into α - and β -tubulin by

1 Neutravidin-gel pull down followed by Western blot with anti- α -tubulin or anti- β -
2 tubulin antibodies. Fig. 6A shows that α - and β -tubulin present in lysates from
3 biotinylated 15d-PGJ₂-treated MCF-7 cells were retained on Neutravidin beads,
4 suggesting that 15d-PGJ₂ is able to react with endogenous α - and β -tubulin in intact
5 MCF-7 cells. To further analyze the *in vivo* association between tubulin and 15d-PGJ₂
6 in the living cell, we performed confocal microscopy analysis of MCF-7 cells treated or
7 not with biotinylated 15d-PGJ₂ for 2 h and stained with anti- α - or anti- β -tubulin. As
8 shown in Fig. 6B, a biotinylated 15d-PGJ₂ network, which colocalized with the
9 endogenous tubulin network was clearly seen. This colocalization is also observed as
10 the cell progresses into the cell cycle (Fig. 6C). These results further suggest a direct
11 binding between 15d-PGJ₂ and the MT network.
12
13
14
15
16
17
18
19
20
21
22
23
24
25
26
27
28

29 *Binding of 15d-PGJ₂ to tubulin.* The above results indicate that 15d-PGJ₂ binds to both
30 α - and β -tubulin, therefore we next analyzed untreated and 15d-PGJ₂-treated
31 microtubules samples by mass spectrometry (MS) to characterize the binding site(s) of
32 15d-PGJ₂ within the tubulin. We used a recently reported approach based on hybrid
33 triple-quadrupole mass spectrometry to find the 15d-PGJ₂-binding site(s) [28].
34
35
36
37
38
39
40
41
42
43

44 We first made the characterization of 15d-PGJ₂ molecule by off line mass
45 spectrometric analysis, and an ion at m/z 317.4 Da, corresponding to the monoisotopic,
46 protonated 15d-PGJ₂ molecule, was observed (Supplementary Fig. 1A). In order to find
47 the main fragments corresponding to single or multiple cleavage sites within the 15d-
48 PGJ₂ molecule, an enhanced product ion experiment was performed (Supplementary
49 Fig. 1B). The most intense fragment ions were selected as potential markers for later
50 precursor ion scanning experiments. The fragment ion at m/z 299.4 Da, out of the seven
51
52
53
54
55
56
57
58
59
60
61
62
63
64
65

1 tested (145.2, 169.2, 183.2, 197.2, 215.4, 281.4, and 299.4), was the signal of choice for
2 precursor ion filtering experiments (Supplementary Fig. 1C). The efficiency of
3
4 precursor ion scanning experiments was lower when using the other seven fragment
5
6 ions present in the MS/MS spectrum from the 15d-PGJ₂ molecule (Supplementary Fig
7
8
9 1C).

10
11
12
13
14 Precursor ion scanning-MS chromatograms of trypsin-digested microtubules from
15 untreated (Fig. 7A, upper panel) or 15d-PGJ₂-treated (Fig. 7A, lower panel) samples
16
17 were analyzed. Although no differential, intense chromatographic peaks were found, an
18
19 exhaustive mass composition chromatographic analysis revealed six time positions (1-6
20
21 in Fig. 7A) along the chromatograms corresponding to differential signals producing the
22
23 15d-PGJ₂-derived fragment ion at m/z 299.4 Da. These time positions marked the
24
25 elution time for differential signals tagged with 15d-PGJ₂ (Fig. 7B), which were only
26
27 present in the 15d-PGJ₂-treated sample, as indicated by the asterisks (Fig. 7B).
28
29
30
31
32
33
34
35

36 MS/MS-based peptide sequencing of differential masses 1, 2, and 4 (Supplementary
37
38 Figs. 2A, 2B, and 2D, respectively) demonstrated that these sequences (353-
39
40 TAVC^{PG}DIPPR-361, 300-NMMAAC^{PG}DPR-308, and 219-
41
42 LTTPTYGDLNHLVSATMSGVTTC^{PG}LR-243, respectively) mapped into β -tubulin,
43
44 while the sequences from differential masses 3 (312-YMACC^{PG}LLYR-320), and 5
45
46 (309-HGKYMACC^{PG}LLYR-320; one missed cleavage at K311; not shown)
47
48 corresponded to α -tubulin-derived peptides (Supplementary Fig. 2C). A comprehensive
49
50 study of the fragmentation spectra from the parent ions corresponding to masses 1-5
51
52 revealed that in all cases the cysteine within the sequence was the 15d-PGJ₂-binding
53
54 residue (superscripted PG-cysteine in text and Supplementary Fig. 2). For peptides 3
55
56
57
58
59
60
61
62
63
64
65

1
2
3
4
5
6
7
8
9
10
11
12
13
14
15
16
17
18
19
20
21
22
23
24
25
26
27
28
29
30
31
32
33
34
35
36
37
38
39
40
41
42
43
44
45
46
47
48
49
50
51
52
53
54
55
56
57
58
59
60
61
62
63
64
65

and 5, only one of the two cysteine residues was modified by 15d-PGJ₂. Differential mass 6 corresponded to the unbound 15d-PGJ₂ dimer, appearing later on the chromatogram due to the highly hydrophobic nature of the molecule.

These results were verified by Multiple Reaction Monitoring (MRM) experiments (Fig. 8). Ions at m/z 644.4, 662.9, 726.4, and 989.9 (corresponding to differential masses 1, 2, 3, and 4, respectively) were isolated and fragmented in untreated and 15d-PGJ₂-treated microtubules samples. As can be observed, only in the 15d-PGJ₂-treated chromatogram, the four differential, intense chromatographic peaks were detected (Fig. 8).

DISCUSSION

1
2 Although it has been clearly established that 15d-PGJ₂ is a potent inducer of cell death
3
4 in many cancer cell lines, including human breast cancer cells, our knowledge of the
5
6 mechanisms of action by which 15d-PGJ₂ causes cell death remains incomplete. In the
7
8 present study, we show that cell death induced by 15d-PGJ₂ in human MCF-7 cells is
9
10 preceded by a marked G₂/M arrest. The cells also displayed morphological features that
11
12 identified a mitotic arrest, specifically in metaphase. Our studies also show that 15d-
13
14 PGJ₂ binds to microtubules, forming a covalent bond with several cysteine residues in
15
16 α - and β -tubulin. Overall these results point to a role of 15d-PGJ₂ in breast cancer cells
17
18 independent of PPAR γ activation and possibly involving a direct binding to tubulin and
19
20 posterior disruption of microtubules. This idea is further substantiated by the fact that
21
22 these effects are not observed in rosiglitazone-treated MCF-7 cells.
23
24
25
26
27
28
29
30
31

32 We have previously demonstrated that 15d-PGJ₂ inhibits proliferation and induces
33
34 cellular differentiation and apoptosis in the breast cancer cell line MCF-7, in part by
35
36 blocking the ErbB receptor signaling pathway [7] and by inducing early mitochondrial
37
38 alterations [8]. Our results suggest that the effects of 15d-PGJ₂ can be, both dependent
39
40 and independent of PPAR γ activation [8, 20, 29]. This is in accordance with the
41
42 description by other groups of PPAR γ -independent pleiotropic effects of 15d-PGJ₂
43
44 responsible for its antiproliferative activity [30, 31]. Our data also indicated a possible
45
46 involvement of the cytoskeleton in this process [8]. Consistent with this idea, in this
47
48 study we demonstrate that 15d-PGJ₂ treatment of MCF-7 cells causes extensive MT
49
50 depolymerization and disruption of the MT network in interphase cells, similar to the
51
52 one observed in cells treated with nocodazole. This effect is probably due to the
53
54 observed in vitro and in vivo binding of 15d-PGJ₂ to, both α - and β -tubulin subunits.
55
56
57
58
59
60
61
62
63
64
65

1
2 Centrosomes abnormalities are hallmarks of various cancers and are found in
3
4 essentially all high-grade cancers and in cell lines derived from tumors [32-37]. These
5
6 anomalies are usually associated with an increase in pericentrin staining and the
7
8 appearance of clusters of pericentrin staining material, which may represent multiple
9
10 centrosomes clumped together at a single pole or an inappropriate accumulation of
11
12 pericentrin. On the contrary, non-tumor tissues present a low level of diffuse staining,
13
14 probably reflecting the modest level of cytoplasmic pericentrin known to be present in
15
16 normal cells, or a single discrete focus of pericentrin [35]. Our results show that, in the
17
18 presence of 15d-PGJ₂, MCF-7 cells exhibited fewer pericentrin foci and pericentrin
19
20 staining was considerable lower than in non-treated cells. Also, the abnormal large
21
22 aggregates of pericentrin seen in control MCF-7 cells, were not observed in 15d-PGJ₂-
23
24 treated cells, indicative of a less transformed phenotype.
25
26
27
28
29
30
31
32
33

34 The ability of 15d-PGJ₂ to block MCF-7 cells in G₂/M phase is consistent with a
35
36 disruption of cytoskeleton via binding to tubulin [38]. Among novel drugs for the
37
38 treatment of advanced breast cancer are those that target microtubules. These drugs
39
40 suppress microtubule dynamics and trigger mitotic arrest at the metaphase/anaphase
41
42 transition [39, 40]. In the presence of these drugs, spindle form and mitosis can progress
43
44 as far as the metaphase/anaphase transition. However, the spindles are completely
45
46 unable to pass the mitotic cell cycle checkpoint and to initiate anaphase movements, or
47
48 do so only after a long period of mitotic arrest. In agreement with this, our results show
49
50 that 15d-PGJ₂ completely blocks the transition to anaphase. Only a few cells appear to
51
52 enter the anaphase state but they are unable to complete the segregation of the
53
54 chromosomes and eventually return to a “metaphase-like” stage afterward they die.
55
56
57
58
59
60
61
62
63
64
65

1
2
3
4
5
6
7
8
9
10
11
12
13
14
15
16
17
18
19
20
21
22
23
24
25
26
27
28
29
30
31
32
33
34
35
36
37
38
39
40
41
42
43
44
45
46
47
48
49
50
51
52
53
54
55
56
57
58
59
60
61
62
63
64
65

There is compelling evidence that tubulin-binding agents such as paclitaxel and the vinca alkaloids kill cancer cells primarily by apoptosis [39, 41]. Because mitotic arrest caused by such agents was frequently found to precede apoptosis, a hypothesis that arrest of the cell cycle at mitosis is the primary stimulus for apoptosis has been widely accepted. For example, apoptosis induced by paclitaxel was found to occur directly after a mitotic arrest or after an aberrant mitotic exit [42, 43]. Nevertheless, some investigators have provided evidence against the involvement of mitotic arrest in apoptosis induction by microtubule-binding agents by demonstrating apoptotic events in other phases of the cell cycle [44, 45]. Apoptosis is not the only mechanism by which cells die following a failed mitosis. Many studies have described a form of cell death called mitotic catastrophe. This form of cell death does not require caspase 9 or 3 and can still occur in the presence of caspase inhibitors such as z-VAD-fmk. In this regard, previous work from our laboratory have shown that the cell death induced by 15d-PGJ₂ in breast cancer cells cannot be completely inhibited by treatment with this caspase inhibitor, albeit caspases are activated in MCF-7 cells treated with this prostaglandin [8]. On the other hand, we could not observe any of the common features attributed to mitotic catastrophe, such as giant non-viable multinucleated cells. 15d-PGJ₂-arrested mitotic MCF-7 cells appear to remain arrested in metaphase from which they subsequently entered a cell death pathway without exiting mitosis. This phenomenon has been previously shown in endothelial cells treated with the tubulin-binding agent combretastin A-4-phosphate [46, 47]. These authors have shown that combretastin A-4-phosphate damages mitotic spindles, arrests cells at metaphase, and leads to the death of endothelial mitotic cells with characteristic G₂/M DNA content.

1
2
3
4
5
6
7
8
9
10
11
12
13
14
15
16
17
18
19
20
21
22
23
24
25
26
27
28
29
30
31
32
33
34
35
36
37
38
39
40
41
42
43
44
45
46
47
48
49
50
51
52
53
54
55
56
57
58
59
60
61
62
63
64
65

MS analyses also demonstrated that 15d-PGJ₂ binds covalently to tubulin and that this binding is probably the cause of microtubule depolymerization in 15d-PGJ₂-treated MCF-7 cells. Our results show that 15d-PGJ₂ binds covalently to at least, four cysteine residues into the α - and β -tubulin moieties, as detected by mass spectrometry. 15d-PGJ₂ is characterized by the presence of a cyclopentenone ring containing an electrophilic carbon (C9), and an electrophilic unsaturated carbonyl group (C13) next to the cyclopentenone ring. These two chemically reactive centers can react covalently by means of Michael's addition reaction with nucleophiles, such as the cysteinyl thiol groups in proteins, to form a covalent adduct which is thought to be irreversible under physiological conditions. Some examples of 15d-PGJ₂ Michael's addition to cysteine residues include PPAR γ (reactive carbon at position 13) and NF- κ B (reactive carbon at position 9) proteins [48].

Tubulin is a heterodimeric protein containing 20 cysteine residues, of which twelve are in the α subunit and eight in the β subunit. Five of these cysteines have been characterized as highly reactive [49]. We have shown here that, at least four of them react with 15d-PGJ₂. Cysteine 305 from β -tubulin is located on the surface of the microtubule near the pore, and probably does not have any effect on microtubule stability. In contrast, cysteines 241 and 356 are located at the inner face, between the GTP and the taxol binding sites, and the binding of 15d-PGJ₂ to these residues could alter the normal curvature of the heterodimer, inducing the microtubule depolymerization. In addition, cysteine 316 from α -tubulin is located in the interphase between an α -subunit and a β -subunit, and, consequently, it is very likely that 15d-PGJ₂-binding to this residue could also interfere in the microtubule assembly. Thus,

1 covalent binding of 15d-PGJ₂ to cysteine residues in microtubules is probably the cause
2 of the observed microtubules depolymerization.
3
4
5

6
7 In summary, our data add a new anti-tumoral role for 15d-PGJ₂ based on the ability
8 to directly binding to cysteine residues in α - and β -tubulin independently of PPAR γ . As
9 a consequence, 15d-PGJ₂ disrupts the MT structure in the cytoplasm of interphase cells
10 and the spindle apparatus of mitotic cells leading to a mitotic arrest at the
11 metaphase/anaphase transition, an accumulation of cells in G₂/M phase, and ultimately
12 breast cancer cell death.
13
14
15
16
17
18
19
20
21
22
23
24
25
26
27
28
29
30
31
32
33
34
35
36
37
38
39
40
41
42
43
44
45
46
47
48
49
50
51
52
53
54
55
56
57
58
59
60
61
62
63
64
65

ACKNOWLEDGMENTS

This work was supported by the Ministerio de Educacion y Ciencia grants SAF2004-06263-CO2-01 and SAF2007-62811 (to A.P.-C) and SAF2004-06263-CO2-02 (to A.S.), and the Fondo de Investigaciones Sanitarias grant PIO40682 (to A.P.-C).

CIBERNED is founded by the Instituto de Salud Carlos III. The authors thank Dr. Alberto Alvarez-Barrientos for his help in the flow cytometry analysis. C.C was a postdoctoral fellow from the Ministerio de Educación y Ciencia of Spain. J.D. is a fellow of the Fondo de Investigaciones Sanitarias de la Seguridad Social.

ABBREVIATIONS

MS, mass spectrometry; MT, microtubules; PPAR γ , peroxisome proliferators-activated receptor γ ; RSG, rosiglitazone; 15d-PGJ₂, 15-deoxy- $\Delta^{12,14}$ -prostaglandin J₂

REFERENCES

- 1
2 [1] Gilroy DW, Colville-Nash PR, Willis D, Chivers J, Paul-Clark MJ, Willoughby DA.
3
4 Inducible cyclooxygenase may have anti-inflammatory properties. *Nature medicine*
5
6 1999;5:698-701.
7
8
9 [2] Negishi M, Katoh H. Cyclopentenone prostaglandin receptors. *Prostaglandins Other Lipid*
10
11 *Mediat* 2002;68-69:611-7.
12
13 [3] Straus DS, Glass CK. Cyclopentenone prostaglandins: new insights on biological activities
14
15 and cellular targets. *Med Res Rev* 2001;21:185-210.
16
17
18 [4] Butler R, Mitchell SH, Tindall DJ, Young CY. Nonapoptotic cell death associated with S-
19
20 phase arrest of prostate cancer cells via the peroxisome proliferator-activated receptor
21
22 gamma ligand, 15-deoxy-delta12,14-prostaglandin J2. *Cell Growth Differ* 2000;11:49-61.
23
24 [5] Clay CE, Namen AM, Atsumi G, Willingham MC, High KP, Kute TE, et al. Influence of J
25
26 series prostaglandins on apoptosis and tumorigenesis of breast cancer cells. *Carcinogenesis*
27
28 1999;20:1905-11.
29
30
31 [6] Nencioni A, Lauber K, Grunebach F, Van Parijs L, Denzlinger C, Wesselborg S, et al.
32
33 Cyclopentenone prostaglandins induce lymphocyte apoptosis by activating the
34
35 mitochondrial apoptosis pathway independent of external death receptor signaling. *J*
36
37 *Immunol* 2003;171:5148-56.
38
39
40 [7] Pignatelli M, Cortes-Canteli M, Lai C, Santos A, Perez-Castillo A. The peroxisome
41
42 proliferator-activated receptor gamma is an inhibitor of ErbBs activity in human breast
43
44 cancer cells. *J Cell Sci* 2001;114:4117-26.
45
46
47 [8] Pignatelli M, Sanchez-Rodriguez J, Santos A, Perez-Castillo A. 15-Deoxy- Δ -12,14-
48
49 prostaglandin J2 induces programmed cell death of breast cancer cells by a pleiotropic
50
51 mechanism. *Carcinogenesis* 2005;26:81-92.
52
53
54 [9] Shimada T, Kojima K, Yoshiura K, Hiraishi H, Terano A. Characteristics of the
55
56 peroxisome proliferator activated receptor gamma (PPARgamma) ligand induced apoptosis
57
58 in colon cancer cells. *Gut* 2002;50:658-64.
59
60
61
62
63
64
65

- 1
2
3
4
5
6
7
8
9
10
11
12
13
14
15
16
17
18
19
20
21
22
23
24
25
26
27
28
29
30
31
32
33
34
35
36
37
38
39
40
41
42
43
44
45
46
47
48
49
50
51
52
53
54
55
56
57
58
59
60
61
62
63
64
65
- [10] Tsubouchi Y, Sano H, Kawahito Y, Mukai S, Yamada R, Kohno M, et al. Inhibition of human lung cancer cell growth by the peroxisome proliferator-activated receptor-gamma agonists through induction of apoptosis. *Biochemical and biophysical research communications* 2000;270:400-5.
- [11] Zander T, Kraus JA, Grommes C, Schlegel U, Feinstein D, Klockgether T, et al. Induction of apoptosis in human and rat glioma by agonists of the nuclear receptor PPARgamma. *Journal of neurochemistry* 2002;81:1052-60.
- [12] Kliewer SA, Lenhard JM, Willson TM, Patel I, Morris DC, Lehmann JM. A prostaglandin J2 metabolite binds peroxisome proliferator-activated receptor gamma and promotes adipocyte differentiation. *Cell* 1995;83:813-9.
- [13] Boyault S, Simonin MA, Bianchi A, Compe E, Liagre B, Mainard D, et al. 15-Deoxy-delta12,14-PGJ2, but not troglitazone, modulates IL-1beta effects in human chondrocytes by inhibiting NF-kappaB and AP-1 activation pathways. *FEBS letters* 2001;501:24-30.
- [14] Ward C, Dransfield I, Murray J, Farrow SN, Haslett C, Rossi AG. Prostaglandin D2 and its metabolites induce caspase-dependent granulocyte apoptosis that is mediated via inhibition of I kappa B alpha degradation using a peroxisome proliferator-activated receptor-gamma-independent mechanism. *J Immunol* 2002;168:6232-43.
- [15] Gilroy DW, Lawrence T, Perretti M, Rossi AG. Inflammatory resolution: new opportunities for drug discovery. *Nat Rev Drug Discov* 2004;3:401-16.
- [16] Castrillo A, Diaz-Guerra MJ, Hortelano S, Martin-Sanz P, Bosca L. Inhibition of IkappaB kinase and IkappaB phosphorylation by 15-deoxy-Delta(12,14)-prostaglandin J(2) in activated murine macrophages. *Mol Cell Biol* 2000;20:1692-8.
- [17] Clay CE, Monjabez A, Thorburn J, Chilton FH, High KP. 15-Deoxy-delta12,14-prostaglandin J2-induced apoptosis does not require PPARgamma in breast cancer cells. *J Lipid Res* 2002;43:1818-28.
- [18] Li L, Tao J, Davaille J, Feral C, Mallat A, Rieusset J, et al. 15-deoxy-Delta 12,14-prostaglandin J2 induces apoptosis of human hepatic myofibroblasts. A pathway involving

oxidative stress independently of peroxisome-proliferator-activated receptors. *J Biol Chem* 2001;276:38152-8.

- [19] Nencioni A, Lauber K, Grunebach F, Brugger W, Denzlinger C, Wesselborg S, et al. Cyclopentenone prostaglandins induce caspase activation and apoptosis in dendritic cells by a PPAR-gamma-independent mechanism: regulation by inflammatory and T cell-derived stimuli. *Experimental hematology* 2002;30:1020-8.
- [20] Martinez B, Perez-Castillo A, Santos A. The mitochondrial respiratory complex I is a target for 15-deoxy-D-12,14-prostaglandin J2 (15d-PGJ2) action. *JLipid Res* 2005.
- [21] Jordan MA, Wilson L. Microtubules as a target for anticancer drugs. *Nature reviews* 2004;4:253-65.
- [22] Pellegrini F, Budman DR. Review: tubulin function, action of antitubulin drugs, and new drug development. *Cancer investigation* 2005;23:264-73.
- [23] Downing KH. Structural basis for the interaction of tubulin with proteins and drugs that affect microtubule dynamics. *Annual review of cell and developmental biology* 2000;16:89-111.
- [24] Wilson L, Panda D, Jordan MA. Modulation of microtubule dynamics by drugs: a paradigm for the actions of cellular regulators. *Cell structure and function* 1999;24:329-35.
- [25] Minotti AM, Barlow SB, Cabral F. Resistance to antimetabolic drugs in Chinese hamster ovary cells correlates with changes in the level of polymerized tubulin. *J Biol Chem* 1991;266:3987-94.
- [26] Bu W, Su LK. Regulation of microtubule assembly by human EB1 family proteins. *Oncogene* 2001;20:3185-92.
- [27] Schneeweiss A, Sinn HP, Ehemann V, Khbeis T, Neben K, Krause U, et al. Centrosomal aberrations in primary invasive breast cancer are associated with nodal status and hormone receptor expression. *International journal of cancer* 2003;107:346-52.
- [28] Buey RM, Calvo E, Barasoain I, Pineda O, Edler MC, Matesanz R, et al. Cyclostreptin binds covalently to microtubule pores and luminal taxoid binding sites. *Nat Chem Biol* 2007;3:117-25.

- 1
2
3
4
5
6
7
8
9
10
11
12
13
14
15
16
17
18
19
20
21
22
23
24
25
26
27
28
29
30
31
32
33
34
35
36
37
38
39
40
41
42
43
44
45
46
47
48
49
50
51
52
53
54
55
56
57
58
59
60
61
62
63
64
65
- [29] Pignatelli M, Cocca C, Santos A, Perez-Castillo A. Enhancement of BRCA1 gene expression by the peroxisome proliferator-activated receptor gamma in the MCF-7 breast cancer cell line. *Oncogene* 2003;22:5446-50.
- [30] Chaffer CL, Thomas DM, Thompson EW, Williams ED. PPARgamma-independent induction of growth arrest and apoptosis in prostate and bladder carcinoma. *BMC Cancer* 2006;6:53.
- [31] Kim EH, Na HK, Kim DH, Park SA, Kim HN, Song NY, et al. 15-Deoxy-Delta12,14-prostaglandin J2 induces COX-2 expression through Akt-driven AP-1 activation in human breast cancer cells: a potential role of ROS. *Carcinogenesis* 2008;29:688-95.
- [32] Badano JL, Teslovich TM, Katsanis N. The centrosome in human genetic disease. *Nature reviews* 2005;6:194-205.
- [33] Sankaran S, Parvin JD. Centrosome function in normal and tumor cells. *J Cell Biochem* 2006;99:1240-50.
- [34] Srsen V, Merdes A. The centrosome and cell proliferation. *Cell Div* 2006;1:26.
- [35] Pihan GA, Purohit A, Wallace J, Knecht H, Woda B, Quesenberry P, et al. Centrosome defects and genetic instability in malignant tumors. *Cancer Res* 1998;58:3974-85.
- [36] Schneeweiss A, Sinn HP, Ehemann V, Khbeis T, Neben K, Krause U, et al. Centrosomal aberrations in primary invasive breast cancer are associated with nodal status and hormone receptor expression. *International journal of cancer* 2003;107:346-52.
- [37] Pihan GA, Purohit A, Wallace J, Malhotra R, Liotta L, Doxsey SJ. Centrosome defects can account for cellular and genetic changes that characterize prostate cancer progression. *Cancer Res* 2001;61:2212-9.
- [38] Schneider Y, Chabert P, Stutzmann J, Coelho D, Fougousse A, Gosse F, et al. Resveratrol analog (Z)-3,5,4'-trimethoxystilbene is a potent anti-mitotic drug inhibiting tubulin polymerization. *International journal of cancer* 2003;107:189-96.
- [39] Jordan MA. Mechanism of action of antitumor drugs that interact with microtubules and tubulin. *Current medicinal chemistry* 2002;2:1-17.

- 1
2
3
4
5
6
7
8
9
10
11
12
13
14
15
16
17
18
19
20
21
22
23
24
25
26
27
28
29
30
31
32
33
34
35
36
37
38
39
40
41
42
43
44
45
46
47
48
49
50
51
52
53
54
55
56
57
58
59
60
61
62
63
64
65
- [40] Wilson L, Jordan MA. Microtubule dynamics: taking aim at a moving target. *Chem Biol* 1995;2:569-73.
- [41] Lin HL, Chang YF, Liu TY, Wu CW, Chi CW. Submicromolar paclitaxel induces apoptosis in human gastric cancer cells at early G1 phase. *Anticancer Res* 1998;18:3443-9.
- [42] Jordan MA, Wendell K, Gardiner S, Derry WB, Copp H, Wilson L. Mitotic block induced in HeLa cells by low concentrations of paclitaxel (Taxol) results in abnormal mitotic exit and apoptotic cell death. *Cancer Res* 1996;56:816-25.
- [43] Woods CM, Zhu J, McQueney PA, Bollag D, Lazarides E. Taxol-induced mitotic block triggers rapid onset of a p53-independent apoptotic pathway. *Mol Med* 1995;1:506-26.
- [44] Huang Y, Johnson KR, Norris JS, Fan W. Nuclear factor-kappaB/IkappaB signaling pathway may contribute to the mediation of paclitaxel-induced apoptosis in solid tumor cells. *Cancer Res* 2000;60:4426-32.
- [45] Miller MC, 3rd, Johnson KR, Willingham MC, Fan W. Apoptotic cell death induced by baccatin III, a precursor of paclitaxel, may occur without G(2)/M arrest. *Cancer Chemother Pharmacol* 1999;44:444-52.
- [46] Nabha SM, Mohammad RM, Dandashi MH, Coupaye-Gerard B, Aboukameel A, Pettit GR, et al. Combretastatin-A4 prodrug induces mitotic catastrophe in chronic lymphocytic leukemia cell line independent of caspase activation and poly(ADP-ribose) polymerase cleavage. *Clin Cancer Res* 2002;8:2735-41.
- [47] Kanthou C, Greco O, Stratford A, Cook I, Knight R, Benzakour O, et al. The tubulin-binding agent combretastatin A-4-phosphate arrests endothelial cells in mitosis and induces mitotic cell death. *Am J Pathol* 2004;165:1401-11.
- [48] Kim EH, Surh YJ. 15-deoxy-Delta12,14-prostaglandin J2 as a potential endogenous regulator of redox-sensitive transcription factors. *Biochem Pharmacol* 2006;72:1516-28.
- [49] Britto PJ, Knipling L, Wolff J. The local electrostatic environment determines cysteine reactivity of tubulin. *J Biol Chem* 2002;277:29018-27.

FIGURE LEGENDS

1
2 Figure 1. Effect of 15d-PGJ₂ and rosiglitazone on cell cycle distribution of
3
4 exponentially dividing MCF-7 cells. The numbers indicate the percentage ± SD of cells
5
6 in each phase of the cell cycle. Cells were exposed to 10 μM 15d-PGJ₂, 30 μM
7
8 rosiglitazone (RSG) or 1 μM nocodazole for 24 h and DNA flow cytometry was
9
10 performed on cells. Data are representative of three independent experiments. *, P <
11
12 0.05; *** P < 0.001.
13
14
15
16
17
18

19 Figure 2. Disruption of microtubules in 15d-PGJ₂-treated MCF-7 cells. (A) Cells were
20
21 treated for 12 h with 1 μM nocodazole, 10 μM 15d-PGJ₂ or 30 μM rosiglitazone (RSG),
22
23 fixed and stained with anti-α-tubulin and anti-pericentrin. DNA was stained with DAPI.
24
25 Scale bar, 10 μm. (B) Polymerized tubulin (P) was differentially extracted from soluble
26
27 (S) tubulin in control, rosiglitazone (RSG)- and 15d-PGJ₂-treated MCF-7 cell lysates
28
29 prepared in a MT-stabilizing buffer. Soluble and polymerized tubulin fractions were
30
31 then analyzed by blotting for α-tubulin. (C) Tubulin bands were quantified by
32
33 densitometric analysis and expressed as a percentage of total tubulin levels. *, P < 0.05.
34
35
36
37
38
39
40
41

42 Figure 3. Treatment of MCF-7 cells with 15d-PGJ₂ perturbs mitotic progression.
43
44 Control (A) and cells treated for 24 h with 15d-PGJ₂ (B) were fixed and stained with
45
46 anti-α-tubulin and anti-pericentrin. DNA was stained with DAPI. Shown are
47
48 representative confocal images of MCF-7 cells mitotic progression. Scale bar, 10 μm.
49
50 (C) Frequency of mitotic stages in control and 15d-PGJ₂-treated MCF-7 cells was
51
52 quantified and expressed as a percentage of total cells. ***, P < 0.001.
53
54
55
56
57
58
59
60
61
62
63
64
65

1
2
3
4
5
6
7
8
9
10
11
12
13
14
15
16
17
18
19
20
21
22
23
24
25
26
27
28
29
30
31
32
33
34
35
36
37
38
39
40
41
42
43
44
45
46
47
48
49
50
51
52
53
54
55
56
57
58
59
60
61
62
63
64
65

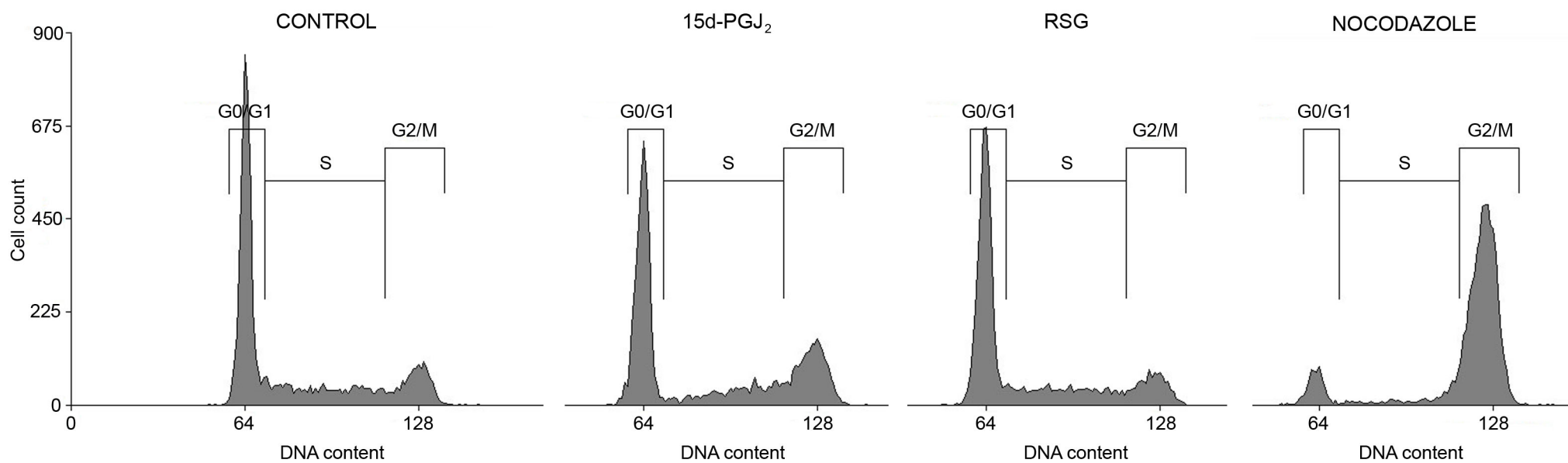
Figure 4. Analysis of mitosis in live MCF-7 cells. Representative images from time-lapse analysis of live cells showing the different phases of mitosis are shown. Time zero, shown in minutes, is the time point at which the nuclear envelope is breakdown and chromatin condensation is evident, just at prophase onset. Cultures were incubated with 10 μM 15d-PGJ₂ or 30 μM rosiglitazone (RSG) and areas were subsequently followed by time-lapse microscopy. Cells treated with 15d-PGJ₂ remained in metaphase for more than 8 h afterward they die. In contrast, non-treated- and rosiglitazone-treated cells escaped mitosis after \sim 1 h. Scale bars, 50 (lower magnification) and 10 (higher magnification) μm . Time-lapse movies for the sequential images shown in this Fig. can be found online.

Figure 5. Effect of 15d-PGJ₂ on tubulin polymerization *in vitro*. Purified bovine brain tubulin was incubated in the presence of buffer (blank), 1 μM nocodazole, 10 μM 15d-PGJ₂, or 200 μM paclitaxel at 37°C, and absorbance readings were recorded at 340 nm each 30 s for 1 h. Data are representative of two independent experiments performed in triplicate.

Figure 6. Binding of biotinylated 15d-PGJ₂ to α - and β -tubulin *in vivo*. (A) MCF-7 cells were incubated or not with biotinylated 15d-PGJ₂ for 2 h and cell lysates were subjected to pull-down assays with Neutravidin-gel beads. The presence of α - and β -tubulin was assessed by Western blot analysis with specific antibodies. (B) MCF-7 cells were treated as in A and cellular accumulation of biotinylated 15d-PGJ₂ was evaluated by confocal microscopy. Tubulin was detected with a specific mouse monoclonal antibody and 15d-PGJ₂ with an anti-biotin antibody. Scale bar, 10 μm . (C) Same staining as in B, showing colocalisation of biotinylated 15d-PG₂ in mitotic cells. Scale bar, 20 μm .

1
2 Figure 7. MS analyses of 15d-PGJ₂ binding to microtubules. Total ion chromatogram
3
4 (TIC) of the precursor ion scanning of fragment at m/z 299.4 from control (A, upper
5
6 panel) or 15d-PGJ₂-treated (A, lower panel) microtubules samples, digested with
7
8 trypsin. Arrows labeled as 1-4 indicate retention times corresponding to different
9
10 peptide mass composition between control and 15d-PGJ₂-treated microtubules samples.
11
12 These differences are detailed in (B) with labels 1-4 indicating the 15d-PGJ₂-modified
13
14 sequences. C means control-, and PG means 15d-PGJ₂-treated microtubules samples.
15
16 Differential masses absent in the control mass spectrum are labeled as an (*). Peaks 5
17
18 and 6 correspond to differential chromatographic peaks. Peak 5 contains the peptide
19
20 with sequence 309-HGKYMACC^{PG}LLYR-320 (one missed cleavage at K311). Peak 6
21
22 corresponds to the 15d-PGJ₂ dimer.
23
24
25
26
27
28
29
30

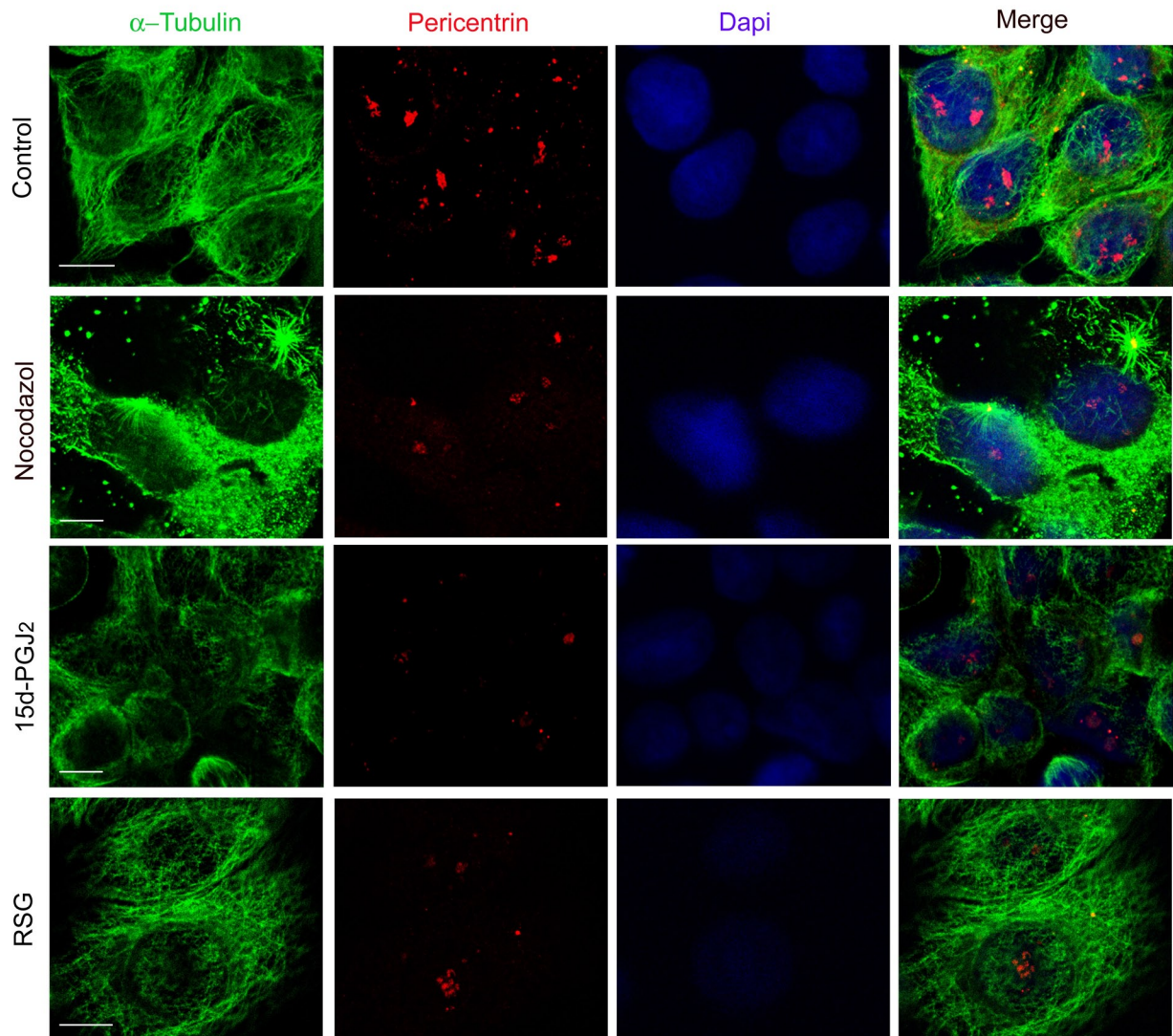
31 Figure 8. MRM experiments with control and 15d-PGJ₂-treated microtubules samples.
32
33 MRM experiments from tryptic, 15d-PGJ₂-modified peptides 1-4. The inset shows the
34
35 MRM results for the corresponding control microtubules sample.
36
37
38
39
40
41
42
43
44
45
46
47
48
49
50
51
52
53
54
55
56
57
58
59
60
61
62
63
64
65



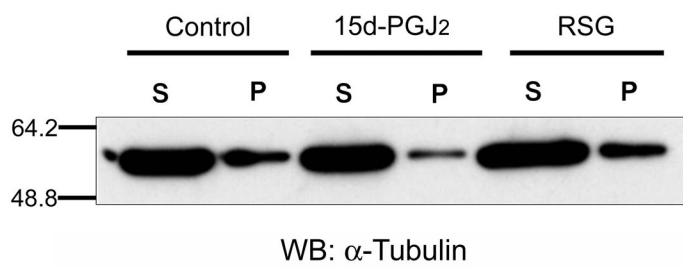
	G0/G1	S	G2/M (%)
Control	55.67 ± 2.52	25.50 ± 1.50	17.10 ± 1.15
15d-PGJ ₂	44.67 ± 5.69 *	15.00 ± 4.36 *	38.33 ± 2.52 ***
RSG	57.44 ± 1.39	21.67 ± 3.51	19.28 ± 3.09
Nocodazole	6.23 ± 3.61 ***	12.26 ± 1.65 *	79.44 ± 1.81 ***

Figure 2

A



B



C

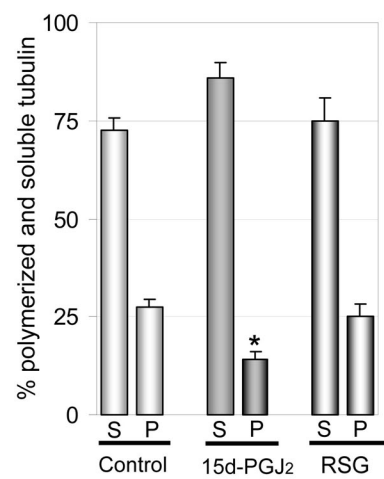
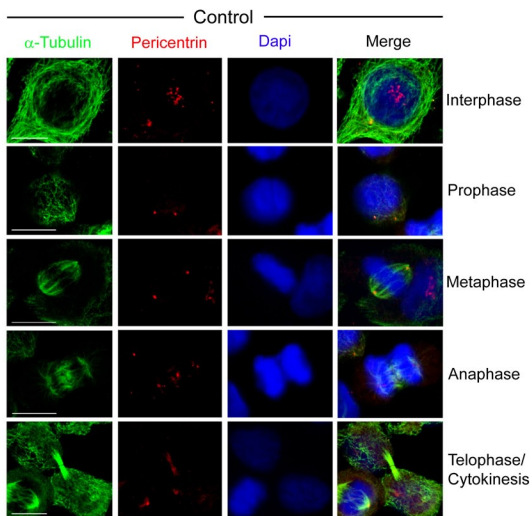
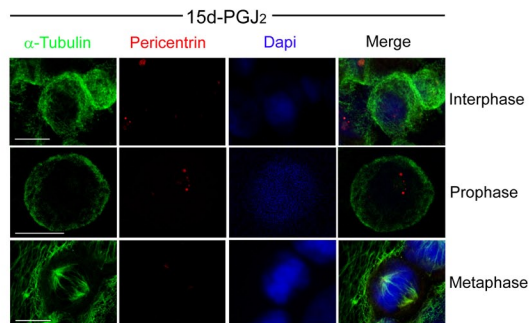


Figure 3

A



B



C

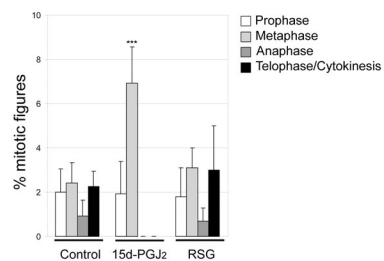


Figure 4

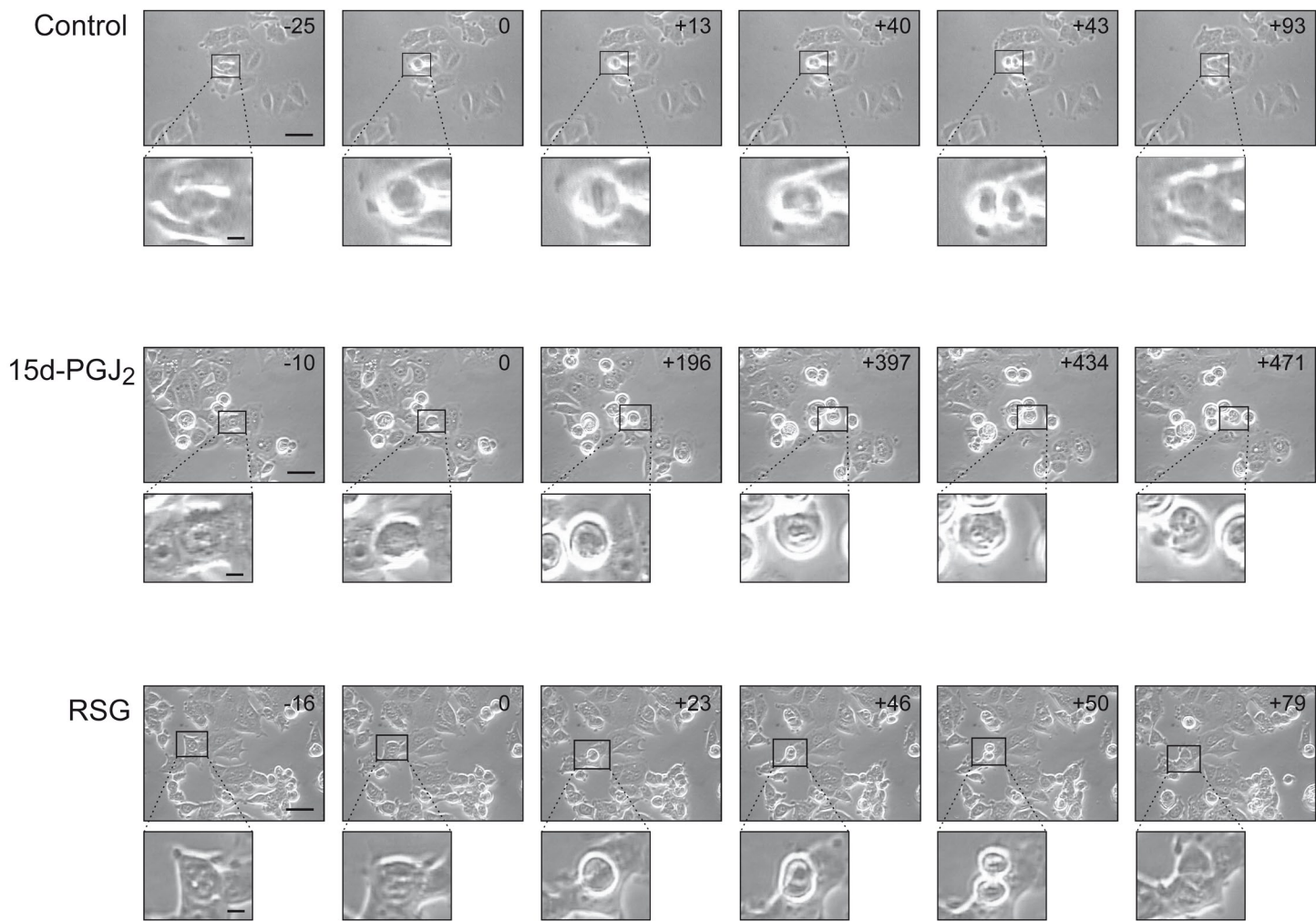


Figure 5

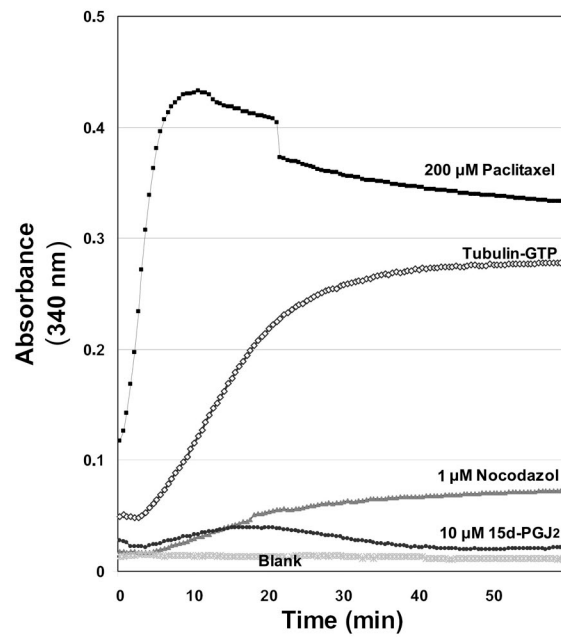
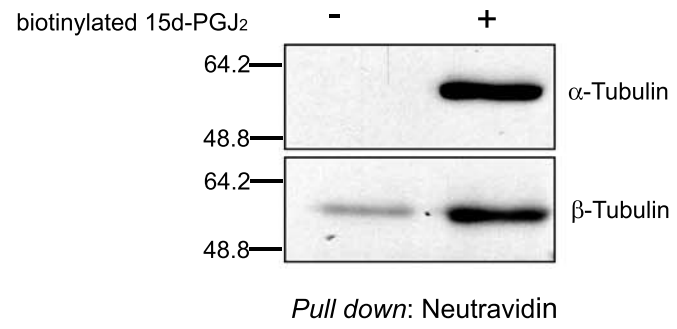
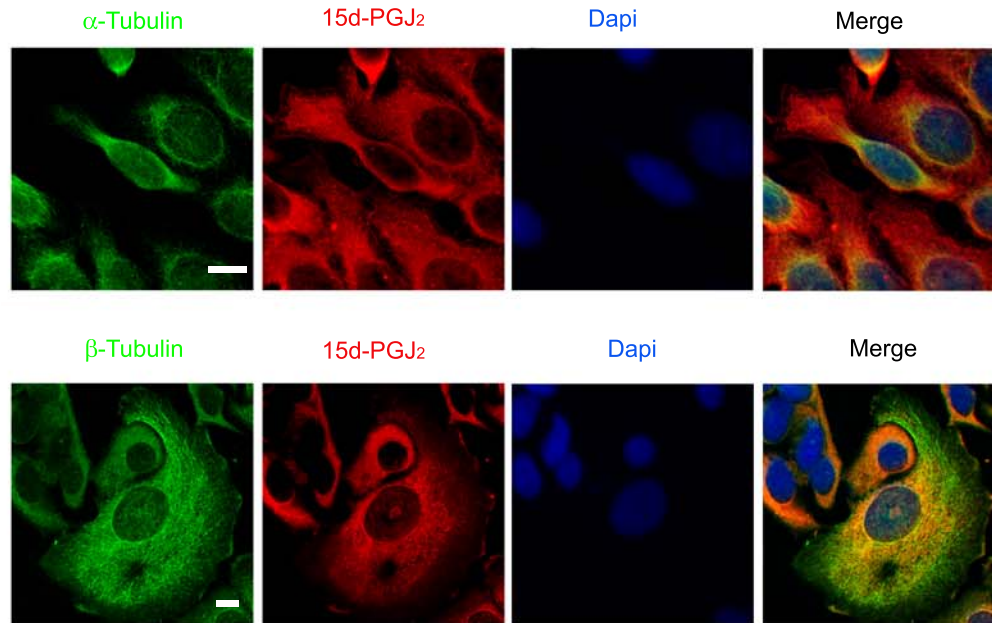


Figure 6

A



B



C

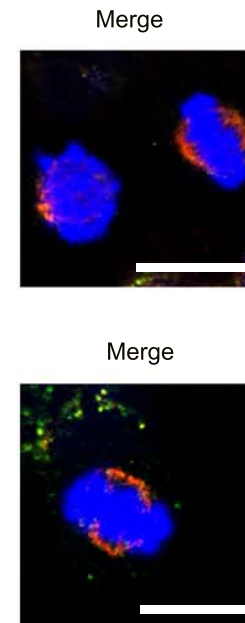


Figure 7

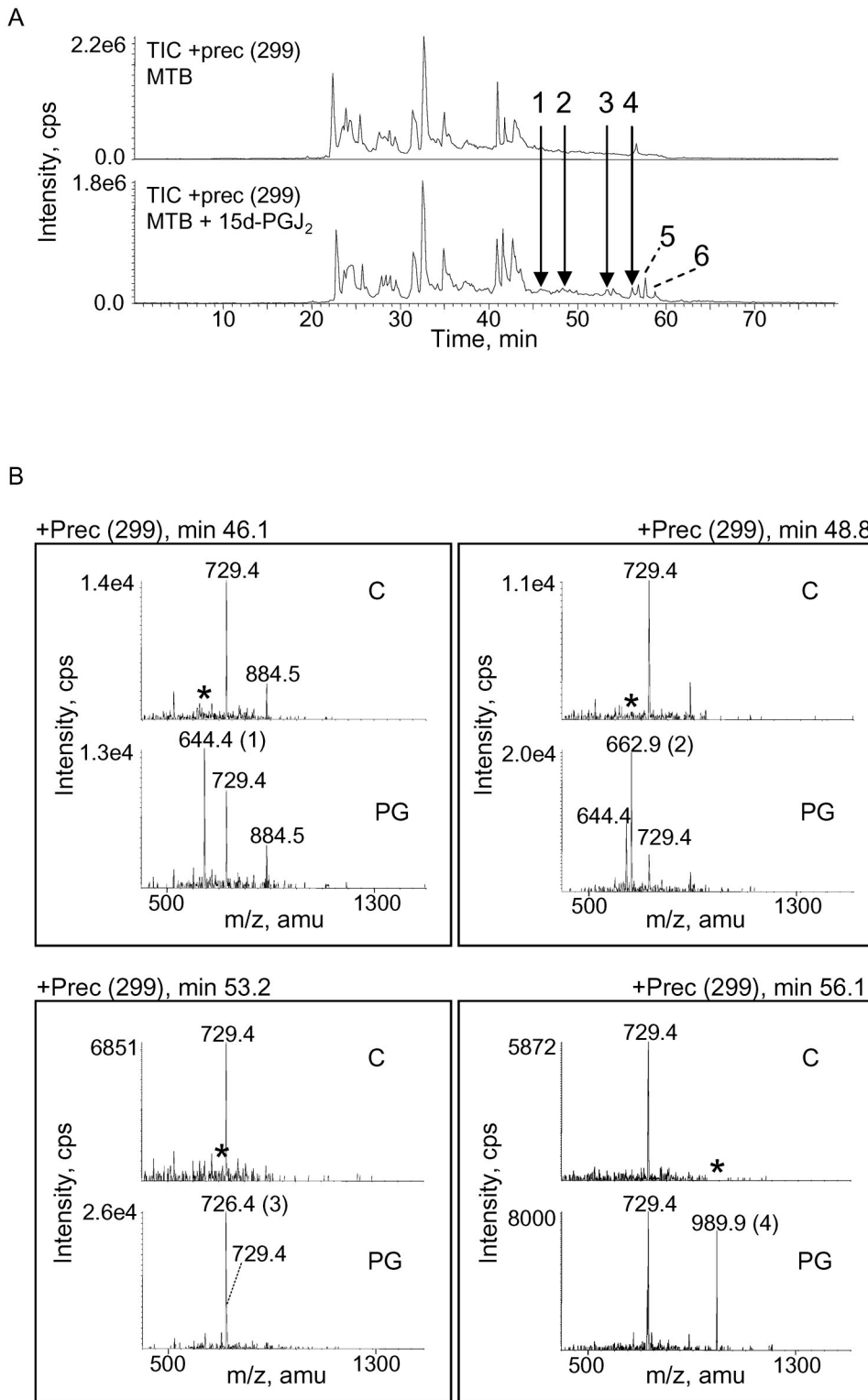
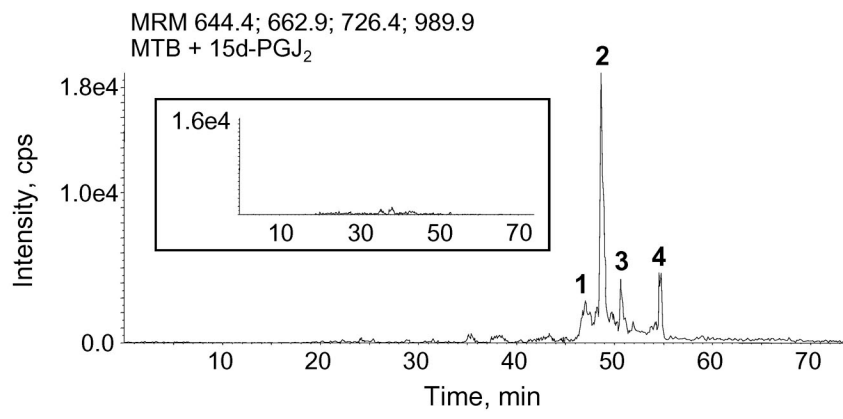


Figure 8



Supplemental Figure 1. *Off line* nanospray characterization of 15d-PGJ₂ by triple quadrupole MS. An ion at m/z 317.3 Da, corresponding to the monoisotopic, protonated 15d-PGJ₂ molecule, was observed (A). In order to find the main fragments corresponding to single or multiple cleavage sites within the 15d-PGJ₂ molecule, an enhanced product ion experiment was performed. The ion at m/z 317.3 Da was isolated and fragmented (B). The most intense fragment ions were selected as potential markers for later precursor ion scanning experiments in order to find the best marker mass to select precursor ions for filtration of peptides that were tagged with 15d-PGJ₂. The fragment ion at m/z 299.4 Da was the signal of choice for precursor ion filtering experiments (C). The efficiency of precursor ion scanning experiments was lower when using other fragment ions present in the MS/MS spectrum from the 15d-PGJ₂ molecule (black arrows) (C).

Supplemental Figure 2. Characterization of 15d-PGJ₂ binding site by triple quadrupole MS. The figure displays the main fragmentation series (carboxy, y, and amino, b, series) for the doubly-charged parent ions from peak 1-3 (A-C, respectively), and for the triply-charged parent ion from peak 4 (D). On each panel the corresponding peptide sequence is shown, as well as fragments containing the 15d-PGJ₂ (superscripted PG). Numbers in boxes (including the filtering mass at m/z 299.4 Da for the precursor ion scanning experiments) indicate masses resulting from fragmentation of the 15d-PGJ₂ molecule. Water loss of some fragments are marked with an (*), and some secondary fragmentation series peptides (a series) are also indicated.

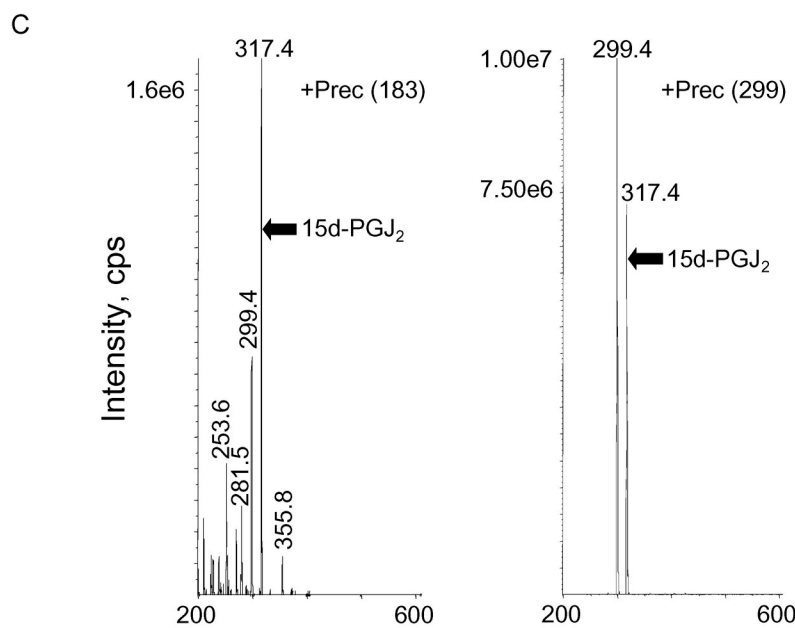
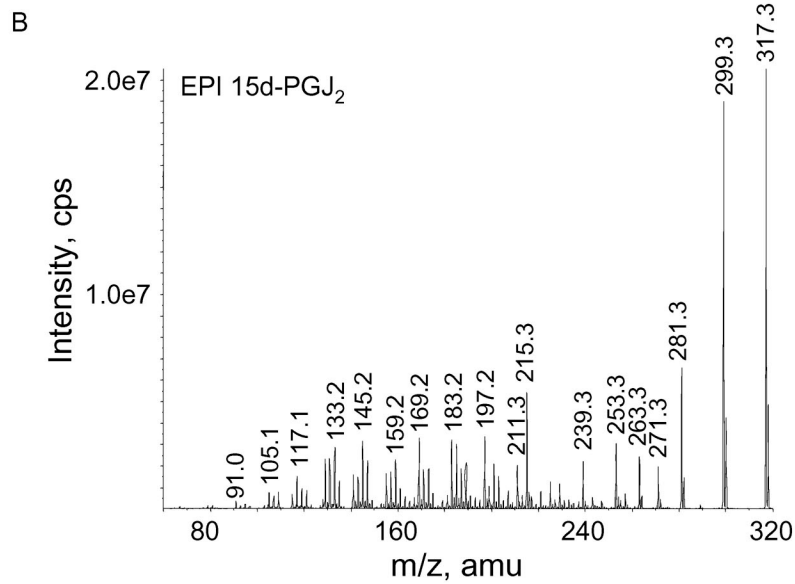
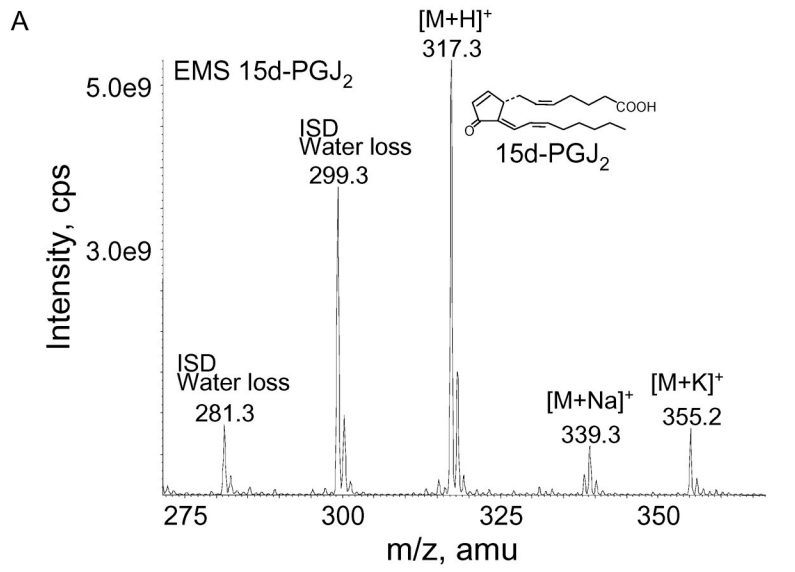
Supplemental Video 1. Mitosis progression in control MCF-7 cells. Time-lapse sequence taken from control MCF-7 cells progressing through mitosis. Images were collected every minute, and the movie runs at 7 frames per second. Bar, 50 μ m. Video corresponds to the cell shown in Figure 4 (two upper panels).

Supplemental Video 2. Mitosis progression in 15d-PGJ₂-treated MCF-7 cells. Time-lapse sequence taken from MCF-7 cells progressing through mitosis in the presence of 15d-PGJ₂. Images were collected every minute, and the movie runs at 7 frames per second. Bar, 50 μ m. Video corresponds to the cell shown in Figure 4 (two middle panels).

Supplemental Video 3. Mitosis progression in rosiglitazone-treated MCF-7 cells

Time-lapse sequence taken from MCF-7 cells progressing through mitosis in the presence of rosiglitazone. Images were collected every minute, and the movie runs at 7 frames per second. Bar, 50 μm . Video corresponds to the cell shown in Figure 4 (two lower panels).

Accepted Manuscript



Supplementary Figure 2

